AGU PUBLICATIONS

Geophysical Research Letters

RESEARCH LETTER
10.1002/2016GL069524

Key Points:
- We map the brine extent, surface density, and roughness over McMurdo Ice Shelf
- Brine horizontal and vertical extent is controlled by snow accumulation
- An echo-free zone might localize scattering from accreted ice or ice platelets

Supporting Information:
- Supporting Information S1

Correspondence to:
C. Grima,
cgrima@ig.utexas.edu

Citation:
Grima, C., J. S. Greenbaum, E. J. Lopez Garcia, K. M. Soderlund, A. Rosales, D. D. Blankenship, and D. A. Young (2016), Radar detection of the brine extent at McMurdo Ice Shelf, Antarctica, and its control by snow accumulation, *Geophys. Res. Lett.*, *43*, 7011–7018, doi:10.1002/2016GL069524.

Received 9 MAY 2016
Accepted 20 JUN 2016
Accepted article online 28 JUN 2016
Published online 13 JUL 2016

Radar detection of the brine extent at McMurdo Ice Shelf, Antarctica, and its control by snow accumulation

Cyril Grima[1], Jamin S. Greenbaum[1], Erika J. Lopez Garcia[1], Krista M. Soderlund[1], Arami Rosales[1,2], Donald D. Blankenship[1], and Duncan A. Young[1]

[1]Institute for Geophysics, University of Texas at Austin, Austin, Texas, USA, [2]Department of Physics, University of Texas at Austin, Austin, Texas, USA

Abstract We derive the surface density and brine infiltration depth/extent at McMurdo Ice Shelf, Antarctica, from combined analysis of radar profiles and radar statistical reconnaissance of the surface from 2011 to 2012 austral summer airborne observations. Most of the brine boundaries appear controlled, directly or indirectly, by the snow accumulation pattern. The infiltration is bounded westward by an ablation area and resides just above the pore close-off depth over most of its extent. The eastern brine limit matches a light-snow corridor, suggesting a reversed pressure gradient at depth that might sharply slow down the infiltration. Brine into ice is confirmed at the deepest locations north and east of Williams Field. The ice-ocean interface is undetected west of the infiltrated zone, except in localized patches. We hypothesize this echo-free zone to be due to high scattering below the surface, possibly from a network of accreted ice and/or ice platelets at the ice-ocean interface.

1. Introduction

The McMurdo Ice Shelf (MIS) is a portion of the Ross Ice Shelf (RIS) bounded by McMurdo sound to the north, White and Black Islands to the south, and the Transantarctic Mountains to the west (Figure 1). Ice is added to the MIS from the east by the RIS and lost through surface ablation to the west and calving to the north [*Glasser et al.*, 2014]. Rapid transitions from basal melting to platelet ice accumulation are known to occur beneath the MIS over short distance scales and time scales [*Robinson et al.*, 2010; *Rack et al.*, 2013], controlled by oceanic exchange between the Western Ross Sea and circulation beneath the RIS [*Robinson et al.*, 2010; *Stern et al.*, 2013]. The ice surface is known for gradients in snowfall [*Heine*, 1967] and impurities [*Glasser et al.*, 2006; *Rack et al.*, 2013]; however, the MIS is perhaps best known for the presence of brine-soaked firn [e.g., *Stuart and Bull*, 1962]. Although brine infiltration is known to occur in several Antarctic ice shelves [e.g., *Dubrovin*, 1962; *Ewen Smith and Evans*, 1971; *Thomas*, 1973], the process has not been discussed in recent literature despite its importance for the development of englacial microbial habitats or for its potential impact on ice shelf stability. While studies to date have confirmed the existence and behavior of brine layers through discrete sampling with ice cores [*Heine*, 1968] and surface radar sounding traverses [e.g., *Kovacs and Gow*, 1975; *Morse and Waddington*, 1994], the active processes that exert primary control on its extent has remained elusive. By combining new techniques for radar-derived surface density/roughness quantification with traditional ice radar sounding, we show brine extent is primarily controlled by local snow accumulation. Here snow accumulation refers to both snowfall and wind-driven snow redeposition.

We investigate the brine with the HiCARS2 (High-Capability Radar Sounder 2) data set acquired over the MIS during the 2011–2012 southern summer for the NASA's Operation IceBridge Project. First, we apply the Radar Statistical Reconnaissance (RSR) technique [*Grima et al.*, 2014b] to the radar surface echo to derive and classify surface properties in terms of density and roughness. We show that this technique is capable of detecting liquid brine when its depth is less than the radar vertical resolution δv (hereinafter referred to near-surface depths). Second, we use the RSR-derived surface density, and an empirical depth-density model is used to obtain the brine depth from the brine echo delay detected in the radar profiles. Based on this new information, we discuss snow accumulation, proxied by the surface density, and its implications for the horizontal and vertical extent of the brine zone.

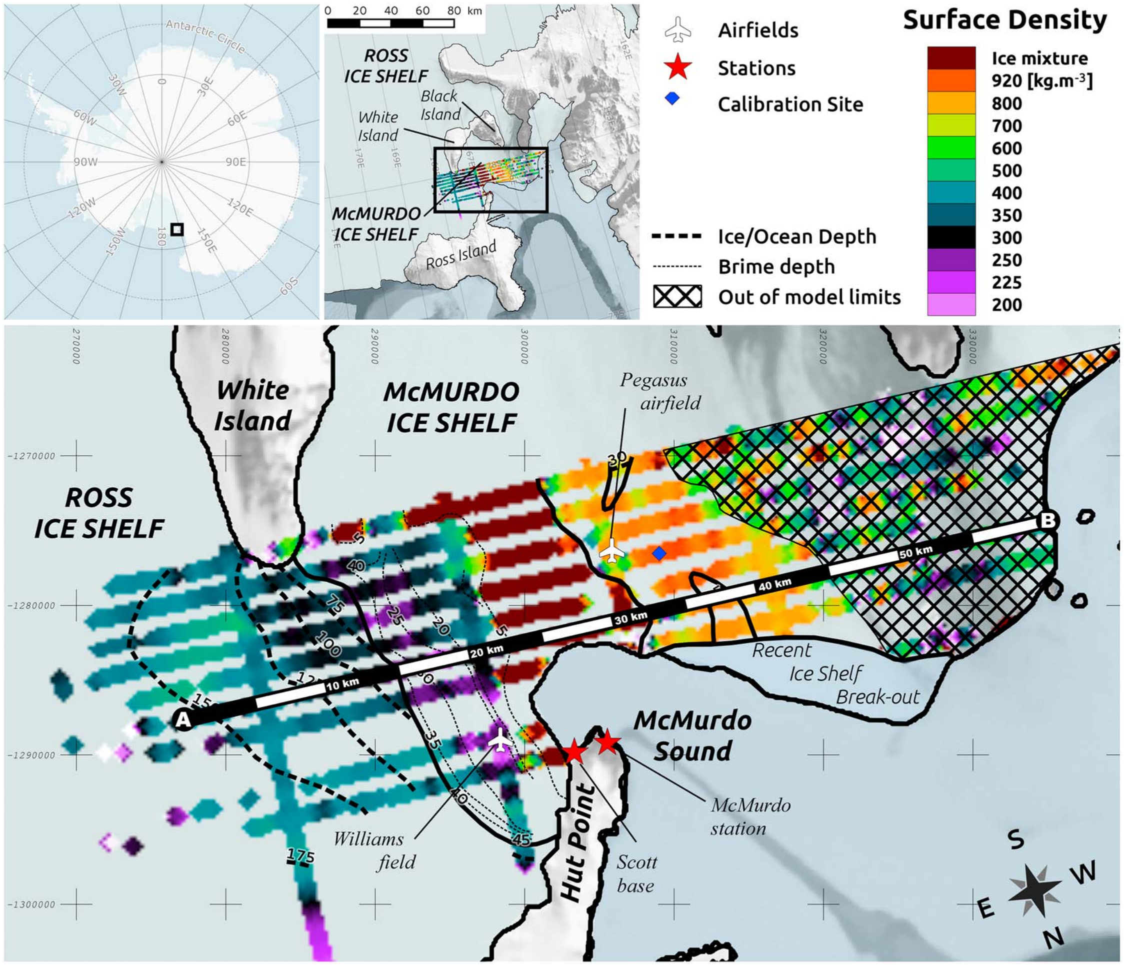

Figure 1. (first panel) Continental and regional maps illustrating the geographic context of McMurdo Ice Shelf (MIS). (second to fifth panels) Surface densities inverted from Radar Statistical Reconnaissance (RSR)-derived permittivities (Figure S6 in the supporting information) and as flown during the 2011–2012 HiCARS2 airborne campaign. “Ice mixtures” indicate a contaminated ice (possibly with liquid water) in the near surface (down to 5–10 m). Ice/ocean interface and brine depths from Figure 3 are superimposed. The AB segment locates the 60 km long profiles in Figure 2.

2. Data and Methods

2.1. Radar Sounder

HiCARS2 is a 60 MHz central frequency (f), 5 m wavelength (l), 15 MHz bandwidth (B), airborne radar sounder maintained and operated by the University of Texas, Institute for Geophysics (UTIG), and flown on board a Basler BT-67. This radar system is similar to HiCARS [*Peters et al.*, 2005] with upgraded components. The surface area illuminated by HiCARS2 is 200 m to 400 m in diameter (pulse-limited footprint) depending on the aircraft altitude. The vertical resolution $\delta v = c/(2B\sqrt{\epsilon})$, where c is the speed of light in vacuum and ϵ the dielectric constant (permittivity) of the sounded material, ranges from $\sim$ 5.6 m in pure ice (ϵ = 3.15) to $\sim$9.5 m in dry snow (ϵ = 1.1) [*Kovacs et al.*, 1995].

2.2. Surface Radar Statistical Reconnaissance

Radar statistical reconnaissance (RSR) characterizes near-surface density and roughness by splitting the received echo energy into its two fundamental components, reflectance and scattering, and inverting them to constrain the physical properties of the target [*Grima et al.*, 2012, 2014a, 2014b]. The reflectance is the amount of signal with a deterministic phase within the total energy (i.e., coherence), while the scattering term accounts for the random phase contribution (i.e., incoherence). When the signal return is from the surface, the reflectance is mostly determined by the surface permittivity (related to its composition and density), while scattering is mainly a function of surface roughness and random internal geometries of the near surface at the wavelength scale.

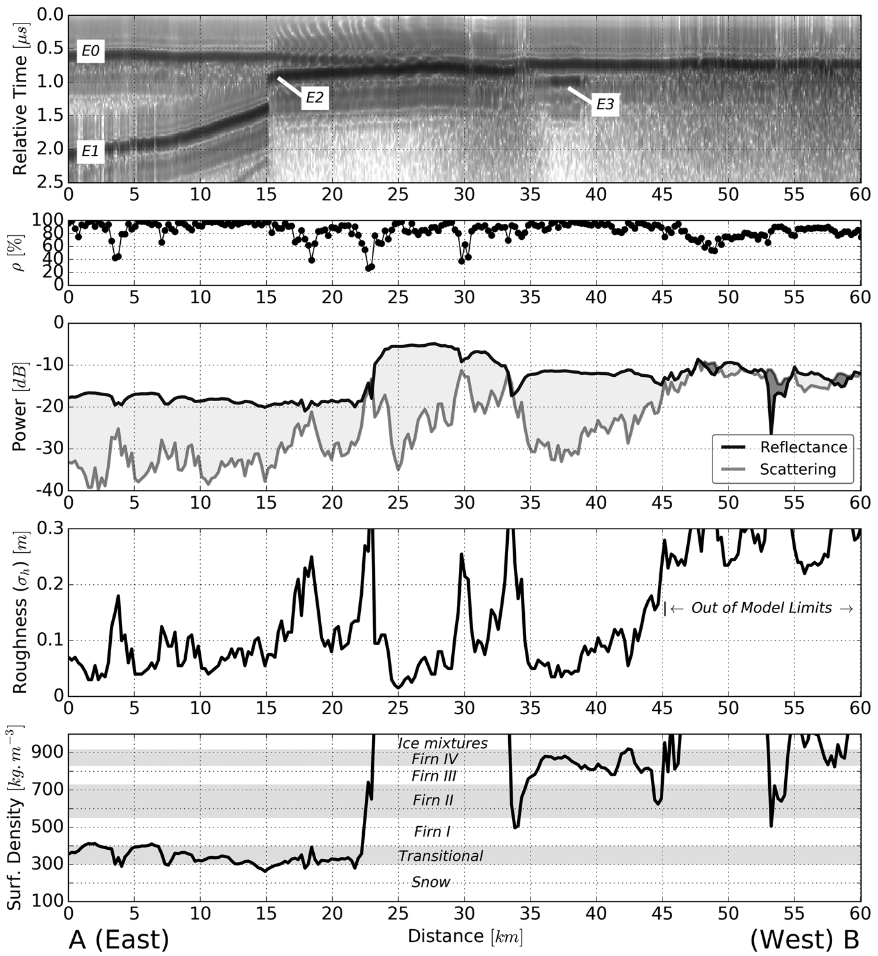

Figure 2. Deep and near-surface properties retrieved by radar along segment AB located in Figure 1. (first panel) The HiCARS2 radargram. E0 labels the surface echo (first return), E1 and E3 represent the ice/ocean interface, and E2 is the brine layer. (second to fifth panels) The parameters derived from the RSR: correlation coefficient of the statistical fit, reflectance/scattering components, surface root-mean-square roughness, and surface density, respectively.

Derivation of both components is obtained by best fitting the amplitude distribution of a set of surface echoes with a theoretical stochastic envelope whose parameters are a function of the reflectance and scattering [*Destrempes and Cloutier*, 2010]. Once both components are deduced from the fit, they are used in a theoretical backscattering model to obtain surface properties [*Ulaby et al.*, 1981]. Here we apply the RSR in the same manner as *Grima et al.* [2014a, 2014b] (see Text S1) to extract the surface root-mean-square heights (σ_h) and permittivity (ϵ). ϵ is then translated into dry-snow density (d) from an empirical relationship [*Kovacs et al.*, 1995; *Frolov and Macheret*, 1999]:

$$d\left[\mathrm{kgm^{-3}}\right] = 1183.432 \cdot \left(\sqrt{\epsilon} - 1\right) \tag{1}$$

2.3. Radar Profiles

The radar signal is reflected/scattered back to the antenna by every dielectric gradient on its propagation path until signal extinction. As the signal is transmitted at high repetition frequency along track, a vertical cross section is built providing subsurface dielectric horizons with a time-delay vertical axis (Figure 2, first panel). The surface-subsurface echo time delay (t) is related to depth (h) through the velocity of light in the medium. A generalized form for a heterogeneous permittivity-depth profile is

$$t = \frac{2}{c}\int_0^h \sqrt{\epsilon(z)}\mathrm{d}z \tag{2}$$

We have inverted h for the second echo below the surface (the surface is labeled E0 in Figure 2, bottom) by finding the solution matching the observed t in (2). ϵ is bounded to d through (1) so that $\epsilon(z)$ can be directly obtained from a depth-density model. In that purpose, we have used Sorge's law, an empirical steady state density profile [*Cuffey and Paterson*, 2010]

$$d(z) = d_i - [d_i - d_s]e^{-1.9z/z_t} \tag{3}$$

where d_i is the density of ice, d_s is the density at the surface as derived from the RSR, and z_t the firn-ice transition depth (where d = 830 kg m^{-3}). z_t is specific to the local climatic conditions. We have considered z_t = 19 m, the shallowest measurement obtained from ice coring by *Kovacs et al.* [1982] at MIS over the brine, and z_t = 60 m, a representative depth for RIS [*Ligtenberg et al.*, 2011]. This conservative range for z_t added to the radar range resolution gives a tight range of uncertainty on the inverted depth between ±5 m and ±6 m, increasing with decreasing surface density. Hence, the 4–5 m brine steps reported by *Kovacs et al.* [1982] cannot be resolved. Brine steps are discontinuities observed in the deepening of brine horizons and characterizing some inland termination of the brine layer. It is usually associated to past brine intrusions triggered by periodic breakouts of the ice shelf.

3. Results

3.1. Surface Radar Statistics

Figure 2 (second to fourth panels) shows the RSR-derived parameters along the 60 km AB segment located in Figure 1 and illustrates the various sets of characteristics observed across MIS (Figures S2–S6). The inverted surface density and roughness from all of the HiCARS2 tracks are shown in Figures 1 and S6, respectively. These have been extrapolated to produce a classification map of surface firn compaction phases overlapped by roughness (Figure 3, top).

Surface properties have an east-west variation pattern. The eastern part overlapping RIS and MIS (0 km to 22 km on segment AB) is smooth (σ_h< 0.10 m) and dominated by 300–400 kg m^{-3} surface densities, characterizing the transitional snow/firn compaction phase [*Cuffey and Paterson*, 2010]. This region is intersected by a corridor of lighter snow (<300 kg m^{-3}) and medium roughness (σ_h= 0.10–0.25 m) extending from the northern extremity of White Island to Hut Point that can be distinguished in Figure 1. This is consistent with high-precipitation rates reported at Williams Field that is located within this corridor [*Mellor*, 1993].

The central part of MIS (22–33 km on segment AB) is characterized by a remarkable −6 dB reflectance similar to $\epsilon \approx 10$. Contaminants can dope the permittivity of ice above 3.15 [*Shabtaie and Bentley*, 1995], but values as high as 10 are only typical of igneous or metamorphic rocks not encountered at this location [*Telford et al.*, 1990]. The alternative is the presence of wet snow/firn. *Geldsetzer et al.* [2009] showed that ϵ for brine-wetted snow increases by a factor of 78.65 times the brine volume fraction. Therefore, we interpret the observed high permittivity as a near-surface soaked firn, presumably an infiltrated brine layer, at a depth lower than HiCARS range resolution (5–10 m) and in such proportion that it dominates the surface echo and masks any surface density information. The brine appears to be bounded to the west by high roughness that could also be partly interpreted as an artifact from substantial volume scattering caused by the brine infiltration process in the near surface. West of the brine zone (33–45 km on segment AB), the near surface is dominated by a smooth and impermeable firn or ice (830–917 kg m^{-3}) characterizing the MIS ablation area [*Mellor*, 1993].

Finally, eastern regions (beyond 45 km on segment AB) have a low reflectance over scattering ratio that prohibits applying RSR to derive confident surface properties (see Text S1). This radar signature covers the Black Island medial moraine and is consistent with the *Glasser et al.* [2006] description of dirty ice largely covered by debris.

3.2. Radar Profiles

Over the RIS, the secondary echo (E1) shallows westward from ~150 m to 75–100 m over a 8–10 km distance. We interpret E1 as the ice-ocean interface with ice thickness transitioning from the relatively thick RIS to the thinner MIS. The secondary echo breaks and shifts upward in a zone nearly aligned with the light-snow corridor between White Island and Hut Point (at 15 km on segment AB in Figure 2). The new secondary echo (E2) shallows westward from 35 to 45 km on segment AB (Figure 2) until merging with E0 (at ~25 km on segment AB). The E2 western limit corresponds with the eastern boundary of near-surface brine detected with

10.1002/2016GL069524

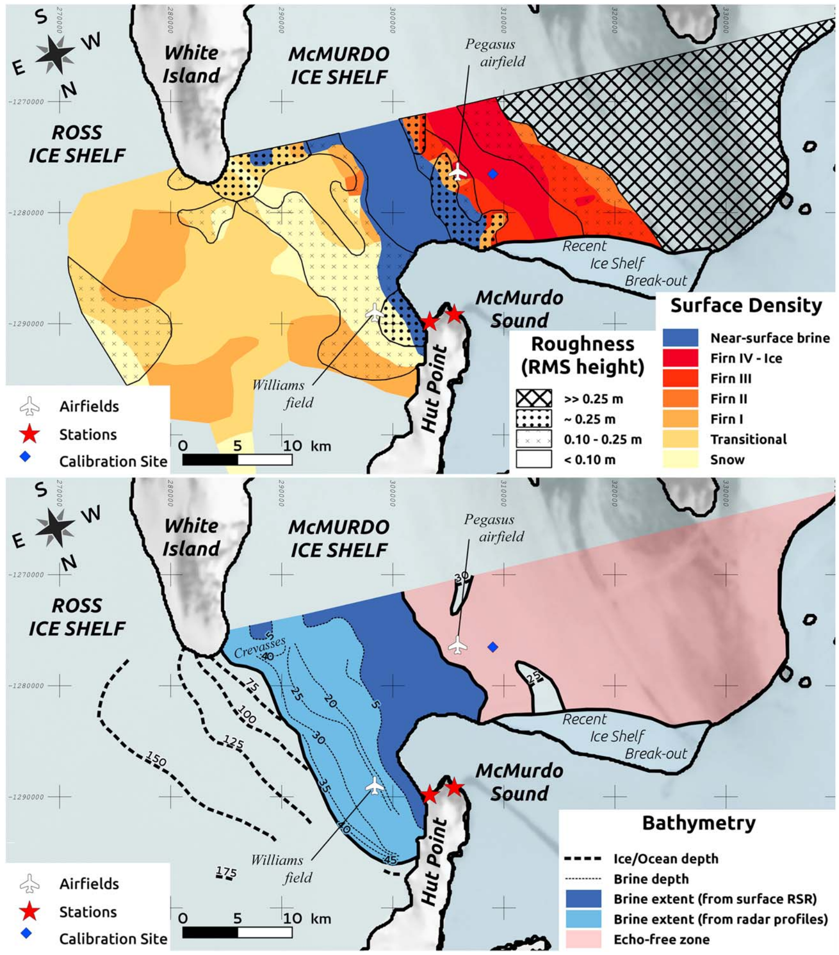

Figure 3. (top) Surface property classification in terms of the RSR-derived roughness and surface density. Snow ($<$300 kg m^{-3}), snow-firn transition (300–400 kg m^{-3}), firn I (400–550 kg m^{-3}), firn II (550–730 kg m^{-3}), firn III (730–830 kg m^{-3}), and firn IV-ice (830–917 kg m^{-3}) are the different compaction phases of dry snow/firn [*Cuffey and Paterson*, 2010]. (bottom) EFZ extent and depth of the brine and ice/ocean interface from radar profile analysis. Depths are given with an uncertainty of $\pm$5–6 m. The RSR-detected brine layer depth is within the radar vertical resolution (5–10 m).

surface RSR (Figure 3, top) so that we interpret E2 as the top of the brine layer. This transition from surface RSR detection to radio-echo imaging confirms that the RSR skin-depth sensitivity is on the order of the radar vertical resolution [*Grima et al.*, 2014a]. Both detections (near-surface brine and E2) form the total brine extent (Figure 3, bottom). The highly reflective brine layer [*Geldsetzer et al.*, 2009] shields the deeper ice/ocean interface from radar detection [e.g., *Kovacs et al.*, 1982].

West of the brine, over both the ablation area and the Black Island medial moraine, is an echo-free zone (EFZ) with no secondary detection except at a few locations (E3). The E3 interface depth (25–30 m $\pm$3 m) is similar to the ice thickness of ~30 m obtained by electromagnetic induction sounding at the same location by *Rack et al.* [2013]. The existence of an EFZ where the ice thickness is expected to be few decameters is puzzling, especially with a 60 MHz radar sounder able to penetrate as deep as 4 km into the Antarctic plateau [*Fretwell et al.*, 2013]. In extreme cases, the signal at the medial moraine could be scattered away from the receiver by high surface roughness, but the terrain configuration does not explain the EFZ extension over the ablation area (e.g., E3), one of the smoothest surfaces of the entire survey. The fact that some detections locally arise within the EFZ while the surface properties do not change is in favor of a spatially widespread, but heterogeneously distributed, extinction process below the surface. Since the ice thickness is only 6 times the HiCARS2 wavelength, a scenario where diffusion is dominant over attenuation is more likely. A thick heterogeneous unit originating from accumulated platelet ice at the ice-ocean interface [*Robinson et al.*, 2010; *Rack et al.*, 2013] could be responsible for signal scattering at the origin of the EFZ.

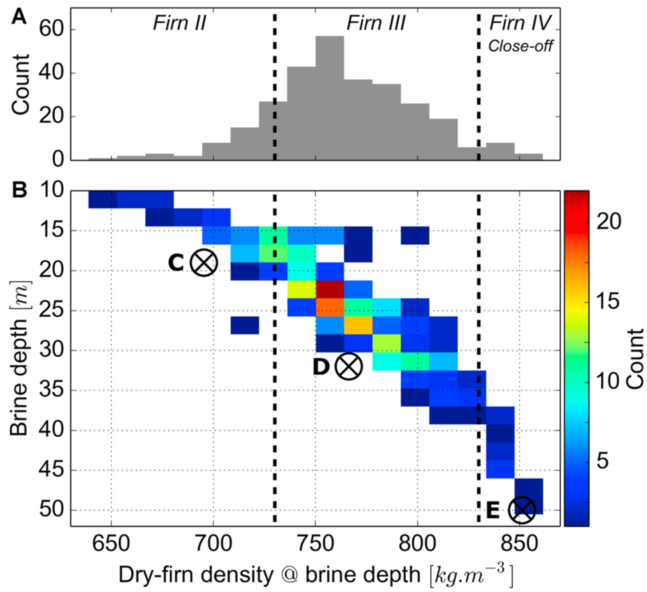

Figure 4. (a) Distribution of the equivalent dry-firn density estimated at depth to the top of the brine layer. Firn-III extends from 730 kg m^{-3} to 830 kg m^{-3}. (b) Same as above broken down with respect to brine depth. The black crossed circles indicate measurements from the ice cores C, D, and E reported by *Kovacs et al.* [1982] just above the brine layer and in the vicinity of Williams field in 1977.

4. Discussion and Conclusion

From $d(z)$ and h derived in section 2.3 we can directly associate the brine layer to a dry-firn density at the same depth (d_h). Figure 4a shows that 80% of our measurements locate the top brine in the 730–830 kg m^{-3} range (firn-III). It demonstrates that brine percolates down and resides mainly in the firn-III layer, the last compaction phase before the impermeable firn-IV. This result confirms early assessments that the firn/ice transition is a major actor in controlling the brine extent [*Kovacs et al.*, 1982]. Figure 4b suggests a relationship between the brine depth and the associated firn density. At shallow depths (<20 m), the top brine overflows the firn-II layer. At deeper depths (>40 m), essentially located north and east of Williams field (see Figure 2), our study indicates the brine is in the firn-IV layer, consistent with the dry-firn density above the brine obtained from ice coring by *Kovacs et al.* [1982] (their Figures 6 and 7) in 1977 (Figure 4). This behavior may arise primarily from progressive compaction of the firn matrix with the overlying snow load and locally from partial dissolution of the ice by concentrated brine in deeper and warmer part of the ice shelf [*Kovacs et al.*, 1982].

Westward, the brine is shallow (<5–10 m) and bounded by a firn/ice transition delimiting the ablation area. Eastward, the brine deepens until it stops propagating where the surface density begins to increase (Figure 1), except where it penetrates the firn-IV layer. In a steady state deposition model, the depth of the iso-density layers are inversely proportional to surface density, so that the impermeable ice limit would start to shallow eastward from the location of the light-snow corridor. In such a configuration, the depth below sea level (h_s) decreases while the distance inland (x) increases. Both combined would suddenly weaken the horizontal pressure gradient $\delta P/\delta x = d_{water} g h_s / x$, where d_{water} is the density of water and g is the gravitational acceleration [*Thomas*, 1975; *Kovacs et al.*, 1982; *Morse and Waddington*, 1994]. $\delta P/\delta x$ proportionally controls the horizontal brine flow velocity through the Darcy's law [*Thomas*, 1975; *Kovacs et al.*, 1982; *Morse and Waddington*, 1994]. Therefore, the line of reversed depth gradient (negative to positive) for the iso-density depth is the place where the brine flow is more likely to equilibrate with the RIS westward flow velocity [*Morse and Waddington*, 1994] and stop the infiltration. Notably, the RIS velocity near MIS has been relatively constant at least between 1997 and 2009 [*Scheuchl et al.*, 2012]. The sloping-upward effect on the iso-density layers at depth should be enhanced by higher surface heights on the RIS side due to an eastward transition from thin to thicker floating ice. Despite the strong correlation of the eastern brine limit with the surface density, we cannot rule out alternatives to explain the brine boundary location. The fact that it is located in the RIS-MIS transition area could argue for a mechanism involving different firn characteristics between the two ice shelves. For instance, the brine could freeze when entering into a putative colder RIS firn. However, the surface velocity field reported by *Glasser et al.* [2014, Figure 1] over the area suggests a junction between RIS and MIS away from the brine boundary, at about 25 km on the AB segment (1) and then bending toward White Island.

The surface density can be regulated by snow accumulation (snowfall and wind-driven redeposition) and seasonal melt-freeze events. However, the later process should create signal scattering from ice lenses in the near surface that is not obvious in Figure S3 at the eastern brine's boundary. Furthermore, the eastern part of the MIS is known to be a dry-snow zone [*Glasser et al.*, 2014]. We conclude that snow accumulation variations are the main mechanism defining the snow surface density pattern in this area. This is also supported by the high-precipitation rates reported at Williams Field [*Mellor*, 1993]. In addition, the correlation between measured firn thicknesses [*Kovacs et al.*, 1982] and our inverted brine depths from a steady state model argue for a somewhat constant accumulation of snow over time. Consequently, we state that snow accumulation controls the lateral firn/ice limits and the topography of iso-density layers at depth. Therefore, it is a key element in setting the brine extent. The light-snow corridor between White Island and Hut Point suggests that the snow accumulation pattern is locked to the surrounded geography, possibly by a topographically controlled local climate. Such a permanent feature would explain why surveys of the eastern brine boundary did not identify substantial displacements over the last decades [*Clough*, 1973; *Kovacs et al.*, 1982; *Morse and Waddington*, 1994]. The only detected brine migration is a ∼800 m inland propagation (out of our horizontal resolution) from 1977 to 1993 that occurred north and east of Williams Field [*Morse and Waddington*, 1994], matching the area where we estimate the brine to infiltrate the firn-IV likely by dissolution and/or snow load-driven compaction.

Brine infiltration within firn layers is believed to enhance fracture deepening in ice shelves and may have contributed to the disintegration of the Wilkins Ice Shelf in West Antarctica [*Scambos et al.*, 2009]. As a result, brine should be included in physical descriptions of ice shelves for accurate forecasting of ice shelf behavior and sea level rise because loss of ice shelves will increase grounded ice mass loss [*De Angelis and Skvarca*, 2003; *Scambos et al.*, 2004]. Brine is also a microbial habitat that represents important locations for the study of terrestrial extremophiles that, to date, has been largely restricted to sea ice [*Thomas and Dieckmann*, 2002]. Therefore, in addition to their importance for processes affecting future sea level, studies of brine-soaked ice shelves represent terrestrial analogs that support future observations of icy moons that may host similar processes, such as Jupiter's moon, Europa.

Acknowledgments
We gratefully acknowledge funding from NASA Operation Ice Bridge (NNX11AD33G), the G. Unger Vetlesen Foundation, the Jackson School of Geosciences, and NASA grant 13-ICEE13-00018 to the Jet Propulsion Laboratory. The data products derived in this study are available by contacting the corresponding author. We thank Stefan Ligtenberg and Brooke Medley for their thoughtful reviews. We also thank Inka Koch for her insightful comments and discussions. This is UTIG contribution.

References

Clough, J. W. (1973), Radio echo sounding: Brine percolation layer, *J. Glaciol.*, *12*(64), 141–143.
Cuffey, K. M., and W. S. B. Paterson (2010), *The Physics of Glaciers*, Elsevier Science, Burlington, Mass.
De Angelis, H., and P. Skvarca (2003), Glacier surge after ice shelf collapse, *Science*, *299*(5579), 1560–1563, doi:10.1126/science.1077987.
Destrempes, F., and G. Cloutier (2010), A critical review and uniformized representation of statistical distributions modeling the ultrasound echo envelope., *Ultrasound Med. Biol.*, *36*(7), 1037–1051, doi:10.1016/j.ultrasmedbio.2010.04.001.
Dubrovin, L. (1962), O rassolakh v shel'fovykh lednikakh [brine in ice shelves], *Sovet. Antarkticheskaia Eksped., Inform. biull.*, *35*, 35–38.
Ewen Smith, B., and S. Evans (1971), Radio echo sounding: Absorption and scattering by water inclusion and ice lenses, *J. Glaciol.*, *11*(61), 133–146.
Fretwell, P., et al. (2013), Bedmap2: Improved ice bed, surface and thickness datasets for Antarctica, *Cryosphere*, *7*, 375, doi:10.5194/tc-7-375-2013.
Frolov, A. D., and Y. Y. Macheret (1999), On dielectric properties of dry and wet snow, *Hydrol. Process.*, *13*(12–13), 1755–1760.
Geldsetzer, T., A. Langlois, and J. Yackel (2009), Dielectric properties of brine-wetted snow on first-year sea ice, *Cold Reg. Sci. Technol.*, *58*(1–2), 47–56, doi:10.1016/j.coldregions.2009.03.009.
Glasser, N., B. Goodsell, L. Copland, and W. Lawson (2006), Debris characteristics and ice-shelf dynamics in the ablation region of the McMurdo Ice Shelf, Antarctica, *J. Glaciol.*, *52*(177), 223–234.
Glasser, N. F., T. Holt, E. Fleming, and C. Stevenson (2014), Ice shelf history determined from deformation styles in surface debris, *Antarct. Sci.*, *26*(6), 661–673, doi:10.1017/S0954102014000376.
Grima, C., W. Kofman, A. Herique, R. Orosei, and R. Seu (2012), Quantitative analysis of mars surface radar reflectivity at 20 MHz, *Icarus*, *220*, 84–99, doi:10.1016/j.icarus.2012.04.017.
Grima, C., D. D. Blankenship, D. A. Young, and D. M. Schroeder (2014a), Surface slope control on firn density at Thwaites Glacier, West Antarctica: Results from airborne radar sounding, *Geophys. Res. Lett.*, *41*, 6787–6794, doi:10.1002/2014GL061635.
Grima, C., D. M. Schroeder, D. D. Blankenship, and D. A. Young (2014b), Planetary landing-zone reconnaissance using ice-penetrating radar data: Concept validation in Antarctica, *Planet. Space Sci.*, *103*, 191–204, doi:10.1016/j.pss.2014.07.018.
Heine, A. J. (1967), The McMurdo Ice Shelf, Antarctica: A preliminary report, *N. Z. J. Geol. Geophys.*, *10*(2), 474–478, doi:10.1080/00288306.1967.10426751.
Heine, A. J. (1968), Brine in the Mcmurdo Ice Shelf, Antarctica, *N. Z. J. Geol. Geophys.*, *11*(4), 829–839, doi:10.1080/00288306.1968.10420755.
Kovacs, A., and A. J. Gow (1975), Brine infiltration in the McMurdo Ice Shelf, McMurdo Sound, Antarctica, *J. Geophys. Res.*, *80*, 1957–1961, doi:10.1029/JC080i015p01957.
Kovacs, A., A. J. Gow, J. H. Cragin, and R. M. Morey (1982), The brine zone in the McMurdo Ice Shelf, *CRREL Rep. 82-89*, US Army Cold Regions Research and Engineering Laboratory, Hanover, N. H.
Kovacs, A., A. J. Gow, and R. M. Morey (1995), The in-situ dielectric constant of polar firn revisited, *Cold Reg. Sci. Technol.*, *23*(3), 245–256, doi:10.1016/0165-232X(94)00016-Q.
Ligtenberg, S. R. M., M. M. Helsen, and M. R. van den Broeke (2011), An improved semi-empirical model for the densification of Antarctic firn, *Cryosphere*, *5*, 809–819, doi:10.5194/tc-5-809-2011.
Mellor, M. (1993), Notes on Antarctic aviation, US Army Cold Regions Research and Engineering Laboratory, Hanover, N. H.
Morse, D., and E. Waddington (1994), Recent survey of brine infiltration in McMurdo Ice Shelf, Antarctica, *Ann. Glaciol.*, *20*(1), 215–218, doi:10.3189/172756494794586952.
Peters, M. E., D. D. Blankenship, and D. L. Morse (2005), Analysis techniques for coherent airborne radar sounding: Application to West Antarctic ice streams, *J. Geophys. Res.*, *110*, B06303, doi:10.1029/2004JB003222.
Rack, W., C. Haas, and P. J. Langhorne (2013), Airborne thickness and freeboard measurements over the McMurdo Ice Shelf, Antarctica, and implications for ice density, *J. Geophys. Res. Oceans*, *118*, 5899–5907, doi:10.1002/2013JC009084.

Robinson, N. J., M. J. M. Williams, P. J. Barrett, and A. R. Pyne (2010), Observations of flow and ice-ocean interaction beneath the McMurdo Ice Shelf, Antarctica, *J. Geophys. Res.*, *115*, C03025, doi:10.1029/2008JC005255.

Scambos, T. A., J. A. Bohlander, C. A. Shuman, and P. Skvarca (2004), Glacier acceleration and thinning after ice shelf collapse in the Larsen B embayment, Antarctica, *Geophys. Res. Lett.*, *31*, L18402, doi:10.1029/2004GL020670.

Scambos, T. A., H. A. Fricker, C. Liu, J. Bohlander, J. Fastook, A. Sargent, R. Massom, and M. Wu (2009), Ice shelf disintegration by plate bending and hydro-fracture: Satellite observations and model results of the 2008 Wilkins ice shelf break-ups, *Earth Planet. Sci. Lett.*, *280*(1), 51–60, doi:10.1016/j.epsl.2008.12.027.

Scheuchl, B., J. Mouginot, and E. Rignot (2012), Ice velocity changes in the Ross and Ronne sectors observed using satellite radar data from 1997 and 2009, *Cryosphere*, *6*(5), 1019–1030, doi:10.5194/tc-6-1019-2012.

Shabtaie, S., and C. R. Bentley (1995), Electrical resistivity sounding of the East Antarctic ice sheet, *J. Geophys. Res.*, *100*, 1933–1954, doi:10.1029/94JB02620.

Stern, A. A., M. S. Dinniman, V. Zagorodnov, S. W. Tyler, and D. M. Holland (2013), Intrusion of warm surface water beneath the McMurdo Ice Shelf, Antarctica, *J. Geophys. Res. Oceans*, *118*, 7036–7048, doi:10.1002/2013JC008842.

Stuart, A., and C. Bull (1962), Glaciological observations on the Ross ice shelf near Scott Base, Antarctica, *J. Glaciol.*, *4*, 399–414.

Telford, W. M., L. P. Gedart, and R. E. Sheriff (1990), *Applied Geophysics*, 2nd ed., Cambridge Univ. Press, Cambridge, U. K.

Thomas, R. (1973), The dynamics of the brunt try of ice shelf brines. Ice shelf, coats land, Antarctica, *Sci. Rep. 79*, Br. Antarct. Surv., Cambridge, U. K.

Thomas, R. H. (1975), Liquid brine in ice shelves, *J. Glaciol.*, *14*(70), 125–136.

Thomas, D. N., and G. S. Dieckmann (2002), Antarctic sea ice—A habitat for extremophiles, *Science*, *295*(5555), 641–4, doi:10.1126/science.1063391.

Ulaby, F. T., R. K. Moore, and A. K. Fung (1981), *Microwave Remote Sensing: Active and Passive*, vol. 1-3, Addison-Wesley, Advanced Book Program, Reading, Mass.